JOURNAL OF ENVIRONMENTAL SCIENCES 136 (2024) 68–80

Available online at www.sciencedirect.com

ScienceDirect

www.elsevier.com/locate/jes

JES JOURNAL OF ENVIRONMENTAL SCIENCES

www.jesc.ac.cn

Atmospheric oxidation capacity and O_3 formation in a coastal city of southeast China: Results from simulation based on four-season observation

Gaojie Chen[1,2,3], *Taotao Liu*[1,2,3], *Jinsheng Chen*[1,2,*], *Lingling Xu*[1,2,*], *Baoye Hu*[4], *Chen Yang*[1,2,3], *Xiaolong Fan*[1,2], *Mengren Li*[1,2], *Youwei Hong*[1,2], *Xiaoting Ji*[1,2,3], *Jinfang Chen*[5], *Fuwang Zhang*[6]

[1] *Center for Excellence in Regional Atmospheric Environment, Institute of Urban Environment, Chinese Academy of Sciences, Xiamen 361021, China*
[2] *Key Lab of Urban Environment and Health, Institute of Urban Environment, Chinese Academy of Sciences, Xiamen 361021, China*
[3] *University of Chinese Academy of Sciences, Beijing 100049, China*
[4] *Minnan Normal University, Zhangzhou 363000, China*
[5] *College of Harbour and Coastal Engineering, Jimei University, Xiamen 361021, China*
[6] *Environmental Monitoring Center of Fujian, Fuzhou 350013, China*

ARTICLE INFO

Article history:
Received 12 September 2022
Revised 22 November 2022
Accepted 22 November 2022
Available online 2 December 2022

Keywords:
Atmospheric oxidation capacity
Radical chemistry
Ozone production
Sensitivity analysis

ABSTRACT

The pollution of atmospheric ozone in China shows an obvious upward trend in the past decade. However, the studies on the atmospheric oxidation capacity and O_3 formation in four seasons in the southeastern coastal region of China with the rapid urbanization remain limited. Here, a four-season field observation was carried out in a coastal city of southeast China, using an observation-based model combining with the Master Chemical Mechanism, to explore the atmospheric oxidation capacity (AOC), radical chemistry, O_3 formation pathways and sensitivity. The results showed that the average net O_3 production rate (14.55 ppb/hr) in summer was the strongest, but the average O_3 concentrations in autumn was higher. The AOC and ROx levels presented an obvious seasonal pattern with the maximum value in summer, while the OH reactivity in winter was the highest with an average value of 22.75 sec^{-1}. The OH reactivity was dominated by oxygenated VOCs (OVOCs) (30.6%-42.8%), CO (23.2%-26.8%), NO_2 (13.6%-22.0%), and alkenes (8.4%-12.5%) in different seasons. HONO photolysis dominated OH primary source on daytime in winter, while in other seasons, HONO photolysis in the morning and ozone photolysis in the afternoon contributed mostly. Sensitivity analysis indicated that O_3 production was controlled by VOCs in spring,

* Corresponding authors.
E-mails: jschen@iue.ac.cn (J. Chen), linglingxu@iue.ac.cn (L. Xu).

https://doi.org/10.1016/j.jes.2022.11.015

autumn and winter, but a VOC-limited and NOx-limited regime in summer, and alkene and aromatic species were the major controlling factors to O_3 formation. Overall, the study characterized the atmospheric oxidation capacity and elucidated the controlling factors for O_3 production in the coastal area with the rapid urbanization in China.

Introduction

Tropospheric ozone (O_3) pollution in urban areas has attracted increasing attention in recent years since it has adverse effect on air quality, agriculture production, and human health (Cohen et al., 2017; Zeng et al., 2019). It is mainly generated through the reaction of volatile organic compounds (VOCs) and nitrogen oxides ($NO_x = NO_2 + NO$) under the sunlight condition (Song et al., 2018; Song et al., 2021). However, it's not easy to alleviate O_3 pollution because of the nonlinear relationship of O_3 with its precursors (Wang et al., 2017). Therefore, it's critical to identify the key atmospheric oxidation process and controlling factors of O_3 pollution.

Atmospheric oxidation capacity (AOC), OH reactivity, and radical chemistry are the main driving force affecting atmospheric O_3 photochemistry (Yang et al., 2020; Yang et al., 2021). The AOC plays an important role in transforming primary gaseous pollutants into secondary ones, reflected as the capacity of removing pollutants through oxidation in the tropospheric atmosphere (Xue et al., 2016; Tan et al., 2019c). As the most active oxidants in the daytime, hydroxyl (OH), hydroperoxy (HO_2), and organic peroxy (RO_2) radicals dominate the daytime oxidation capacity of the atmosphere, initiating and participating in a series of photochemical oxidation processes. Generally, photolysis of nitrous acid (HONO), O_3, formaldehyde (HCHO) and other oxygenated VOCs (OVOCs), as well as ozonolysis of unsaturated VOCs were considered as the primary sources of RO_x radicals (Xue et al., 2016; Zhu et al., 2020; Liu et al., 2022b), accelerating the radical recycling to produce O_3. However, primary radical sources changed in different observational campaigns/seasons, related to the intensity of pollutant emissions, pollutant types, and photolysis rates of RO_x precursors locally. For instance, in urban regions in Hongkong, HONO photolysis is the most important source of OH throughout the daytime, and the strength of O_3 photolysis can be not neglected at noon, but photolysis of OVOCs was the predominant sources of HO_2 and RO_2 radicals during the O_3 pollution episode in summer (Xue et al., 2016). In Shanghai, HO_x primary sources in the daytime were HONO photolysis in the morning, and O_3 photolysis in the afternoon in summer and autumn (Zhu et al., 2020). RO_x radicals in Tokyo were dominated by photolysis of HONO in the morning, OVOCs photolysis at midday in summer (Kanaya et al., 2007), but in New York, HONO photolysis was dominant in the daytime in winter (Ren et al., 2006). For the radical sinks, the reactions of RO_x and NOx (e.g., $OH + NO_2$, $RO_2 + NO$ and $RO_2 + NO_2$) were the most important under higher concentrations of NOx; in contrast, the reactions of RO_x and RO_x (e.g., $HO_2 + HO_2$, $RO_2 + HO_2$ and $RO_2 + RO_2$) are the major sinks of radicals under lower concentrations of NO_x (Zhu et al., 2020; Yang et al., 2021).

For O_3 production, it is important to assess O_3 responses to its precursor changes. In urban regions, O_3 production tended to be controlled by VOCs, but a NOx-limited regime in rural areas (Tan et al., 2019a; Wang et al., 2020; Li et al., 2022). However, O_3 production sensitivity varied temporally and spatially due to it was mainly affected by VOC and NOx emissions (Wang et al., 2020). Hence, determining O_3 production sensitivity regimes should be examined case by case. As for VOC groups, aromatics and alkenes were the major VOC groups to O_3 formation (Li et al., 2019), and the necessary control measures on the related VOC emissions should be taken.

Currently, the studies of O_3 photochemistry have been extensively conducted in the North China Plain (NCP), Sichuan Basin (SCB), the Yangtze River Delta (YRD), the Pearl River Delta (PRD) (Tan et al., 2019c; Zhu et al., 2020; Liu et al., 2021; Qu et al., 2021; Wang et al., 2022b). For instance, a study with three cases for different O_3 levels in summer and autumn in YRD, analyzed the AOC, radical budget (Zhu et al., 2020). During a photochemical smog episode in autumn in PRD, Xue et al. explored the oxidative capacity and radical chemistry (Xue et al., 2016; Li et al., 2018b). Besides, during a photochemical polluted episode in late summer and early autumn in four Chinese megacities, Tan et al. studied the influence of oxidative capacity on secondary pollution (Tan et al., 2019c). However, the time span of these studies concentrated in a certain pollution episode or special season, lack of the longer time of field observation, such as four seasons in a year. Moreover, few studies focused on oxidative capacity and O_3 production in coastal regions of southeast China with lower O_3 precursor levels (Liu et al., 2022b).

In recent years, O_3 concentrations have kept increasing in coastal cities of southeast China, and O_3 has become the major pollutants to affect air quality. Ningde is a coastal city in the northeast of Fujian Province of southeast China, located in the middle of the YRD and PRD. The prosperity of sea-port in Ningde promotes the rapid development of economy and industry, making pollutant emissions increased. The weather in Ningde belongs to subtropical monsoon climate with significant seasonal changes, affecting the seasonal pattern of pollutants. Given the differences in pollutant emissions and meteorological conditions in four seasons, it is vital to investigate the variation characteristics of the atmospheric oxidation capacity and the controlling factors of O_3 pollution in four seasons in this coastal city of southeast China.

In this study, a four-season field observation was conducted from 1 January to 28 December in 2019 at an urban site of Ningde, using the observation-based model to analyze the atmospheric oxidation capacity and O_3 production pathways and sensitivity. This study aims to (1) compare seasonal variation characteristics of O_3 and its precursors; (2) characterize the photochemical reactivity; (3) dissect key pathways and

species of O_3 production in four seasons. This study might enhance the understanding of the photochemical pollution and O_3 production in different seasons, as well as the measures to reduce O_3 pollution in coastal area with the rapid urbanization.

1. Materials and methods

1.1. Observation site

The observation was conducted from 1 January to 28 December in 2019 in the Meteorological Bureau (119.53°N, 26.66°E) in Ningde, a coastal city in the northeast of Fujian Province of southeast China (Fig. 1). The observation site is set on the roof of a four-story building about 2 km from the main traffic road, surrounded by mixed commercial and residential areas without direct pollutant emissions. Therefore, it is a typical urban site used for intensive observations of air quality in Ningde. In this study, the time span of spring, summer, autumn, and winter was from 1 March to 31 May, from 1 June to 31 August, from 1 September to 30 November, from 1 January to 28 February and from 1 December to 28 December, respectively.

1.2. Instruments

A gas chromatography system equipped with a mass spectrometer and flame ionization detector (GC-MS/FID) with one-hour time resolution was used to measure VOC species. VOC samples were captured through an ultralow temperature system after H_2O and CO_2 were removed. After thermal desorption, the GC analysis system was utilized. The temperature program duration was 24.5 min, with an initial temperature of 40°C and a final temperature of 180°C. The FID connected to an Al_2O_3/Na_2SO_4 PLOT (50 m × 0.32 mm × 8 μm) column was used to quantify the low-carbon (C2-C5) VOC species and the high-carbon (C5-C12) VOC species (including oxygenated volatile organic compounds (OVOCs) and hydrocarbons) were quantified using MS connected to a DB-1 (30 m × 0.25 mm × 1.0 μm) column. Daily calibration was performed every day at 23:00 using 4 ppb standard mixtures to ensure quantitative accuracy. Internal standard gases (chlorobenzene, bromochloromethane, 1,4-dichlorobenzene, and fluorobromobenzene) were also daily calibrated to ensure the stability of the instrument. The method detection limit (MDL) and relative standard deviation (RSD) of measured VOC species (including alkanes, alkenes, alkynes, aromatics, OVOCs, halocarbons) are listed in Table S1. Additionally, CO, SO_2, O_3, and NO_x (NO/NO_2) were monitored by commercial gas analysis instruments (Thermo Fisher Scientific 48*i*, 43*i*, 49*i*, and 42*i*, respectively, USA). Meanwhile, O_3 was detected using the UV absorption method; a pulsed fluorescence SO_2 analyzer was used to measure SO_2; CO was analyzed with the infrared absorption spectroscopy method; a chemiluminescence NO_x analyzer was used to detect NO_x. The meteorological parameters, including atmospheric pressure (P), air temperature (T), relative humidity (RH), wind speed (WS), wind direction (WD), and ultraviolet (UV) radiation were obtained. The detailed performances of different instruments are summarized in Table S2. All data were used after applying strict data quality control.

1.3. Observation-based model

The observation-based model incorporating Master Chemical Mechanism version 3.3.1 (OBM-MCM) was used to simulate the atmospheric oxidation process and O_3 production sensitivity. Detailed description and parameter settings about

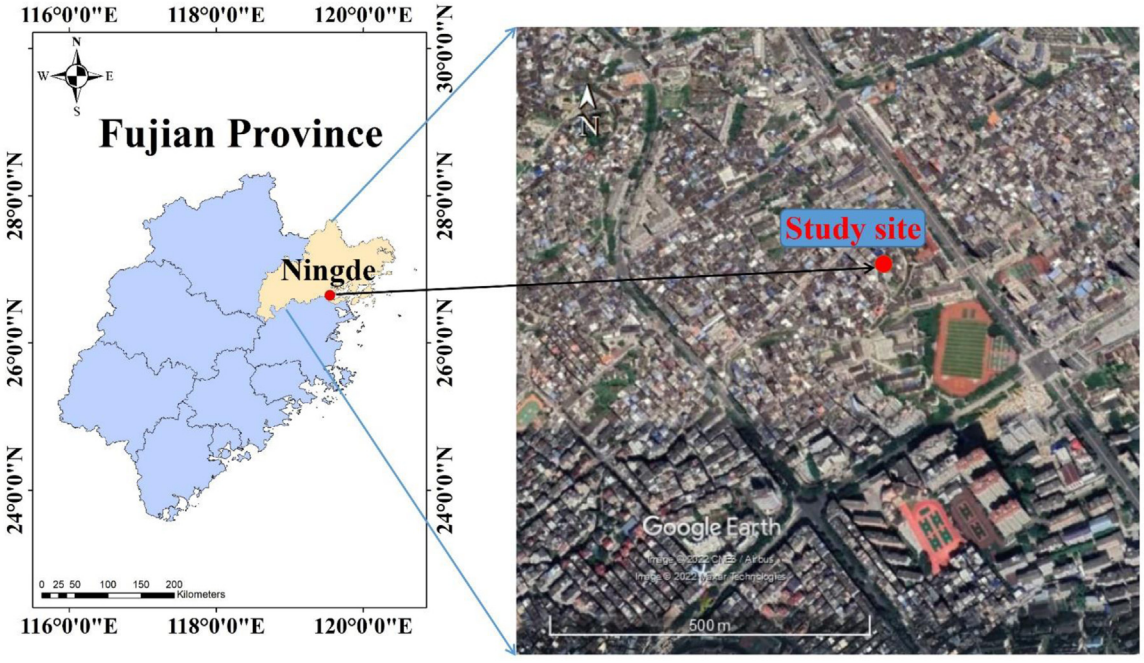

Fig. 1 – The observation site in Ningde in the northeast of Fujian Province. (The topographic image was provided by Google Earth.)

the OBM were illustrated in previous study (Liu et al., 2022a; Liu et al., 2022b). Briefly, the MCM involved methane (CH_4) and 142 non-methane VOC species, and described about 20,000 elementary reactions (Saunders et al., 2003). In order to avoid the continuous accumulation of pollutants in the model, the physical process including dry deposition and the effect of dilution conditions within the boundary layer height was considered. Specially, the effect of dilution mixing in this study was considered for all species by introducing a dilution factor, defined as a function of the change in the planetary boundary layer (PBL) height. The PBL height was assumed to vary from 300 m at night to 1500 m at noon. Before the beginning of the simulation, we ran the model for 5 days to initialize the unconstrained compounds and radicals. The model was constrained by trace gases (e.g., NO, NO_2, SO_2, O_3, CO, VOCs), meteorological parameters, and photolysis rates. In this study, photolysis rates were calculated using the Tropospheric Ultraviolet and Visible Radiation (TUV) model (http://cprm.acom.ucar.edu/Models/TUV/), according to the reported approach (Wang et al., 2018b; Lyu et al., 2019; Liu et al., 2021). The information of the geographical location and study time periods, along with default aerosol optical depth (AOD), cloud optical depth (COD), surface albedo and other parameters, were used to initialize the calculated UV radiation. Then, the COD value was adjusted until the difference between the calculated and observed UV radiation value was less than 1%. The model performance was analyzed in supporting information, comparing observed O_3 concentrations with stimulated O_3 concentrations (Fig. S1). The IOA values of 0.92, 0.85, 0.82, 0.96 in spring, summer, autumn, and winter, respectively, indicated that the result of the OBM-MCM model performance was acceptable. During some study periods, simulated O_3 concentrations were higher than observed O_3 concentrations, likely because the model does not consider the horizontal and vertical transport processes (Lyu et al., 2016).

Generally, the HO_2 + NO and RO_2 + NO reactions are considered as the major O_3 production pathways (Eq. (1)), and the O_3 loss pathways (Eq. (2)) include NO_2 + OH/RO_2, O_3 photolysis, O_3 + OH, O_3 + HO_2, O_3/NO_3 + VOCs. The net O_3 production rate is equivalent to the O_3 production rate minus the O_3 loss rate (Eq. (3)).

$$P(O_3) = k_1[HO_2][NO] + \sum (k_2[RO_2][NO]) \quad (1)$$

$$\begin{aligned} L(O_3) = {} & k_3[O_1D][H_2O] + k_4[O_3][OH] + k_5[O_3][HO_2] \\ & + k_6[NO_2][OH] + \sum (k_7[O_3][VOCs]) \\ & + 2\sum (k_8[NO_3][VOCs]) \end{aligned} \quad (2)$$

$$P_{net}(O_3) = P(O_3) - L(O_3) \quad (3)$$

where, k_i stands for the rate constant.

The relative incremental reactivity (RIR) was usually used to evaluate O_3 production sensitivity, calculated using Eq. (4).

$$RIR = \frac{\Delta P(O_3)/P(O_3)}{\Delta X/X} \quad (4)$$

where, $\Delta P(O_3)/P(O_3)$ represents the relative changes of O_3 production rates; $\Delta X/X$ represents the reduction proportion of O_3 precursors (anthropogenic VOCs (AHC), biogenic VOCs (BHC), NO_x, and CO), adopted as 20%.

1.4. Evaluation of AOC and OH reactivity

The AOC is evaluated by the sum of simulated oxidation rates of CO, CH_4, and VOCs via reactions with OH, NO_3 and O_3 (Yang et al., 2020), calculated by Eq. (5).

$$AOC = \sum_i k_{Y_i}[Y_i][X] \quad (5)$$

where, $[Y_i]$ is the concentrations of reduced substances (VOCs, CO, and CH_4), $[X]$ is the concentrations of oxidants (OH, NO_3, and O_3), and k_{Y_i} is the reaction rate constant of Y_i and X. Notably, the definition of AOC does not include NOx because itis the major OH sinks (Yang et al., 2021).

In addition, the OH reactivity is used to assess loss rates of different reactants (such as VOCs, HONO, SO_2, CO, NOx and HNO_3) with OH radical, equivalent to the inverse of the OH radical lifetime (Yang et al., 2020; Yang et al., 2021), calculated by Eq. (6)

$$k_{OH} = \sum_i k_{OH+X_i}[X_i] \quad (6)$$

where, $[X_i]$ is the concentrations of reactants (VOCs, NO_2, CO etc.), and k_{OH+Xi} represents the corresponding reaction rate constant.

2. Results and discussion

2.1. Overview of observations

The observed time series of meteorological parameters and major pollutant levels in four seasons in 2019 are shown in Fig. 2, and average values with standard deviation of these measured parameters are summarized in Table S3. The average UV radiation (22.56 ± 30.21 W/m^2) and temperature (27.58 ± 3.44 °C) in summer were the highest, followed by autumn (20.02 ± 28.83 W/m^2, 22.45 ± 5.72 °C, respectively) and spring (19.29 ± 27.86 W/m^2, 18.34 ± 5.01°C, respectively), and the lowest in winter ((10.75 ± 18.27) W/m^2, (12.54 ± 3.57)°C, respectively). The highest value of RH was in summer (84.65% ± 11.38%), followed by spring (79.47% ± 15.14%), winter (78.19% ± 15.06%), autumn (72.05% ± 17.36%). The moderate wind speed was in spring ((1.35 ± 0.87) m/sec), summer ((1.39 ± 0.82) m/sec), and autumn ((1.43 ± 0.73) m/sec), but lower wind speed ((1.14 ± 0.71) m/sec) was in winter. Meteorological conditions would directly affect the variation of pollutant concentrations. In summer, higher wind speed, higher temperature and stronger UV accelerated the diffusion and removal of primary pollutants, resulting in the minimum pollutant levels. In contrast, in winter, adverse meteorological conditions, such as static wind speed, lower boundary layer height, lower air temperature and UV, limited the ability of pollutants to spread and remove, caused higher concentrations of primary pollutants. Indeed, NO_x, SO_2, CO concentrations in winter was the highest, followed by spring, autumn, and summer.

Total VOCs showed significant seasonal characteristics with higher concentrations in winter (36.45 ± 23.96 ppb),

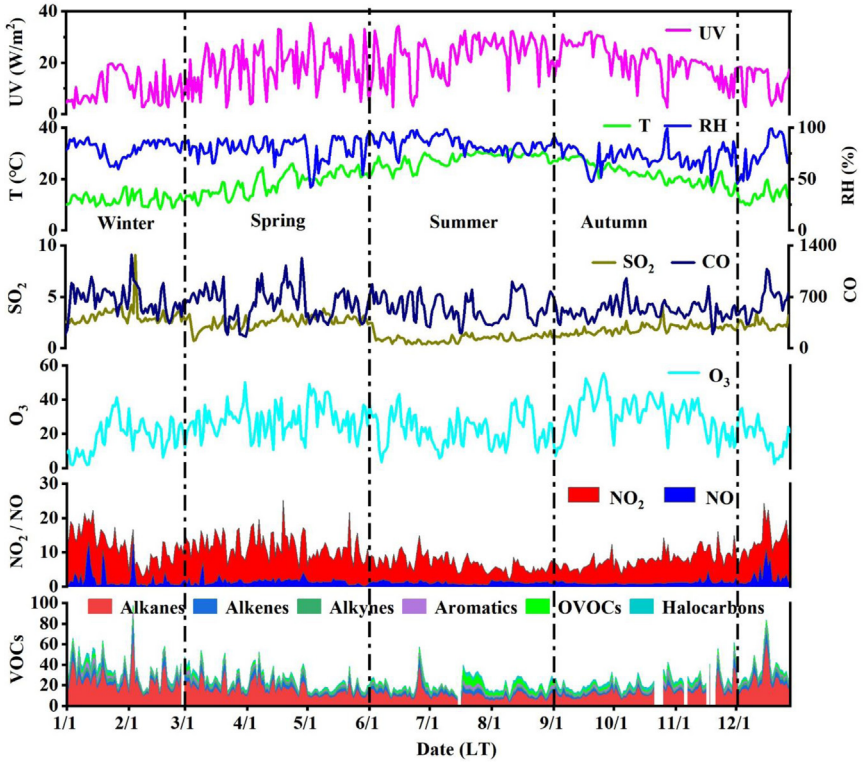

Fig. 2 – Time series of major meteorological parameters and gaseous pollutant levels (Units: ppbv) at this observation site from 1 January to 28 December in 2019.

medium concentrations in spring (24.99 ± 16.63 ppb) and autumn (22.40 ± 13.36 ppb), lower concentrations in summer (19.96 ± 9.82 ppb), in coincidence with seasonal variations of other primary gaseous pollutants. As for VOC groups, alkanes accounted for 59.9% in spring, 47.8% in summer, 54.3% in autumn, and 61.1% in winter of the concentrations of total VOCs, attributing to their widespread emission sources and life span (Song et al., 2018; Zhao et al., 2020). The contributions of alkene to the total VOC concentrations were the second important at the urban site in four seasons (11.2%-13.1%). Compared to other seasons, the levels of OVOCs in summer were the largest, likely due to higher atmospheric oxidation capacity in summer, promoting the secondary formation of OVOCs.

However, the seasonal pattern of O_3 was obviously different from primary pollutants, with higher in autumn and spring, lower in summer and winter in 2019, similar with other cities in Fujian Province in the southeast of China (Liu et al., 2022b), where the influence of the Asian monsoon system on O_3 was significant (Zhang et al., 2013; Wang et al., 2018a). In summer, the collective effect of clean oceanic inflow and frequent precipitation caused lower O_3 concentrations than those in spring. In autumn, when the summer monsoon retreated and the winter monsoon began, the continental outflow enriched with O_3 precursors from the mainland and coupled with strong solar radiation, provided favorable conditions for O_3 generation and accumulation (Zhang et al., 2013). In winter, lower concentrations of O_3 were due to the titration effect of higher NO levels and adverse photochemical reaction conditions (e.g., lower UV).

The average diurnal profiles of O_3 and its precursor concentrations, and meteorological parameters are displayed in Fig. S2. Surprisingly, the concentrations of NOx and VOC groups presented typical diurnal variations in four seasons, higher concentrations in the morning and evening rush hours, indicating that the study site were greatly affected by traffic emissions. The concentrations of NO_x and VOCs were the lowest at noon when stronger WS, higher UV might accelerate the dilution and transformation of primary pollutants. However, the diurnal pattern of O_3 is characterized by the highest concentrations in the afternoon due to stronger UV and a lower titration effect. Except for the influence of the intensity of pollutant emissions and meteorological factors, seasonal differences of the concentrations of measured species were related to the atmospheric oxidation capacity.

2.2. *Characteristics of atmospheric oxidation capacity*

2.2.1. *Seasonal variations of AOC*

The average AOC in the daytime (06:00-18:00 LT) in spring, summer, autumn, and winter was (4.85 ± 3.01) × 10^7, (9.99 ± 4.73) × 10^7, (5.75 ± 3.63) × 10^7, and (2.30 ± 1.60) × 10^7 mol/(cm^3·sec), respectively. The maximum AOC was up to 9.00 × 10^7 mol/(cm^3·sec) in spring, 15.93 × 10^7 mol/(cm^3·sec) in summer, 10.74 × 10^7 mol/(cm^3·sec) in autumn, and 4.52 × 10^7 mol/(cm^3·sec) in winter, respectively. The result showed the AOC levels were the highest in summer, the moderate levels in autumn and spring compared to the lowest levels in winter, indicating higher removal rates of primary pollutants in summer. In contrast, in winter, lower

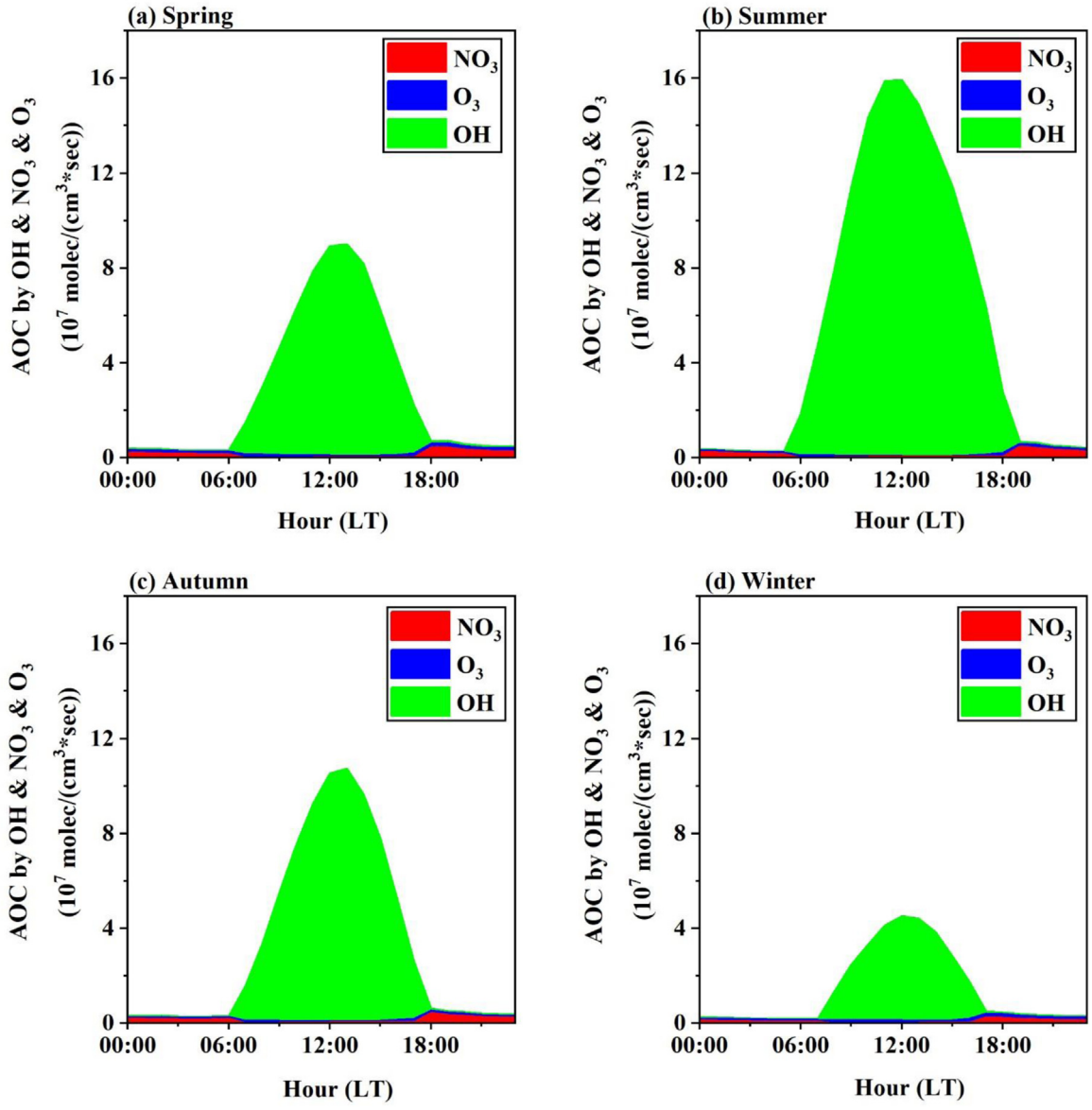

Fig. 3 – Simulated atmospheric oxidation capacity at this observation site in different seasons. (a) Spring, (b) Summer, (c) Autumn, (d) Winter.

AOC levels were not favorable to deplete primary pollutants. The maximum AOC at the urban site was compared to that in Xiamen (1.3×10^8 mol/(cm^3·sec)), in Shanghai (8.8×10^7 mol/(cm^3·sec)), but lower than that in Santiago (3.2×10^8 mol/(cm^3·sec)) and Tung Chung in Hong Kong (2.04×10^8 mol/(cm^3·sec)), and higher than that in Berlin (1.4×10^7 mol/(cm^3·sec)) (Geyer et al., 2001; Elshorbany et al., 2008; Xue et al., 2016; Li et al., 2018b; Zhu et al., 2020; Liu et al., 2022b). The spatial and temporal variations of the AOC were mainly affected by the levels of atmospheric oxidants (e.g., OH, O_3 and NO_3), photochemical reaction conditions (such as solar radiation), pollutant concentrations (Liu et al., 2022b).

The average diurnal variations of the AOC in four seasons are shown in Fig. 3. The AOC exhibited obvious diurnal variation characteristics in different seasons, with the highest levels at midday and lower intensity at night, similar with the diurnal variation of stimulated RO_x levels. The daytime AOC was dominated by OH (96.5% in spring, 99.0% in summer, 97.3% in autumn, and 92.3% in winter). However, NO_3 (56.4%, 65.1%, 61.1%, and 43.2%, in spring, summer, autumn, and winter, respectively) played the leading role in the nighttime AOC, followed by O_3 (28.8%, 21.7%, 23.0%, and 39.9%, respectively), and OH (14.8%, 13.2%, 15.9%, and 16.9%, respectively). Compared to other time of the day, the contribution of NO_3 to the AOC was the most significant at 19:00 LT in summer likely due to the higher abundance of NO_2 promoted the formation of NO_3 under the condition of lower solar radiation at this time. Similar results were found at 18:00 LT in spring, at 18:00 LT in autumn, at 17:00 LT in winter, respectively. Different from previous studies (Xue et al., 2016; Liu et al., 2022b), the contribution of O_3 to the nighttime AOC can be not negligible at the study site because the influence of O_3 on the

AOC is mainly through the ozonolysis of alkenes, the levels of which were abundant at the site, only lower than alkane levels. Overall, OH dominated the AOC in the daytime and NO_3 was the most predominant oxidant at night, indicating the importance of atmospheric oxidants for the AOC, in accordance with reported studies (Xue et al., 2016; Li et al., 2018a; Zhu et al., 2020; Liu et al., 2022b). Notably, previous studies showed that the reactive chlorine radical produced by photolysis of halogen species, such as nitryl chloride and Cl_2, might also play an important role for the AOC in the daytime (Liu et al., 2017; Peng et al., 2022), but these species were not detected in the present study. Therefore, the AOC in this study may be underestimated. Given the importance of OH radical on the daytime AOC, the further analysis of the loss rates of OH radical with different recants needed to be elucidated.

2.2.2. *Characteristics of OH reactivity*

The mean OH reactivity was (18.53 ± 1.67), (15.30 ± 1.98), (15.15 ± 2.00), and (22.75 ± 2.87) sec^{-1}, with a range of 15.92-21.02, 11.88-18.75, 11.86-19.10 and 18.93-28.67 sec^{-1} in spring, summer, autumn and winter, respectively. Obviously, the OH reactivity in winter was the largest, followed by spring, summer and autumn. The OH reactivity in four seasons was lower than that in summer in Xianghe (28 sec^{-1}) in BTH (Yang et al., 2021), in autumn in Heshan (31 sec^{-1}) and in summer in Backgarden (50 sec^{-1}) in PRD (Lou et al., 2010; Yang et al., 2017), mainly due to lower pollutant emissions in our study area. The average diurnal profiles of the OH reactivity (Fig. S3) showed that the OH reactivity was the lowest in the afternoon and the highest in the morning and evening peak hours in four seasons, related to increased primary pollutant emissions from transportation activities (Tan et al., 2019c).In particular, the average OH reactivity in the afternoon rush hour (18:00 LT) in winter presented the highest value, reflecting the highest CO, VOCs, and NOx concentrations at this time.

The contributions of different reactants to the total OH reactivity are compared in Fig. 4. VOCs (including alkanes, alkenes, aromatics, and OVOCs) contributed more than 50% to the total OH reactivity. Meanwhile, OVOCs was the most abundant OH reactant, contributing 33.0% in spring, 42.8% in summer, 38.1% in autumn, 30.6% in winter to the total OH reactivity, implying the importance of OVOCs in the process of radical chemistry and O_3 formation. The related studies indicated that OVOCs can be a large contributor to RO_x radical and O_3 production (Qu et al., 2021; Wang et al., 2022a). The largest contribution of OVOCs to the total OH reactivity was in summer, related with the strongest AOC and the highest concentrations of OVOCs in summer. Besides, the contribution of alkenes to the OH reactivity could be not ignored at the urban site, 9.4% in spring, 8.6% in summer, 8.4% in autumn, and 12.5% in winter. CO (23.2%-26.8%) and NO_2 (13.6%-22.0%) were the major contributors of inorganic compounds to the OH reactivity. For VOC species, their OH reactivity was comparable to those in other Chinese cities (Table S4) (Xu et al., 2011; Yang et al., 2017; Tan et al., 2018b; Yang et al., 2020; Yang et al., 2021), and HCHO, acrolein, ethylene was the predominant contributors to the OH reactivity in different seasons in Ningde. The contributions of NO_2 in winter and spring were higher due to higher levels of NO_2 at the two seasons compared to other seasons. Overall, at the urban site, OVOCs, CO, NO_2 were the most important contributors to the OH reactivity in four seasons. However, in Chinese megacities, such as Beijing, Shanghai, Guangzhou, and Chongqing, NOx (28.0%-35.0%) were considered as the most important OH recants, followed by CO (17.0%-25.0%) and

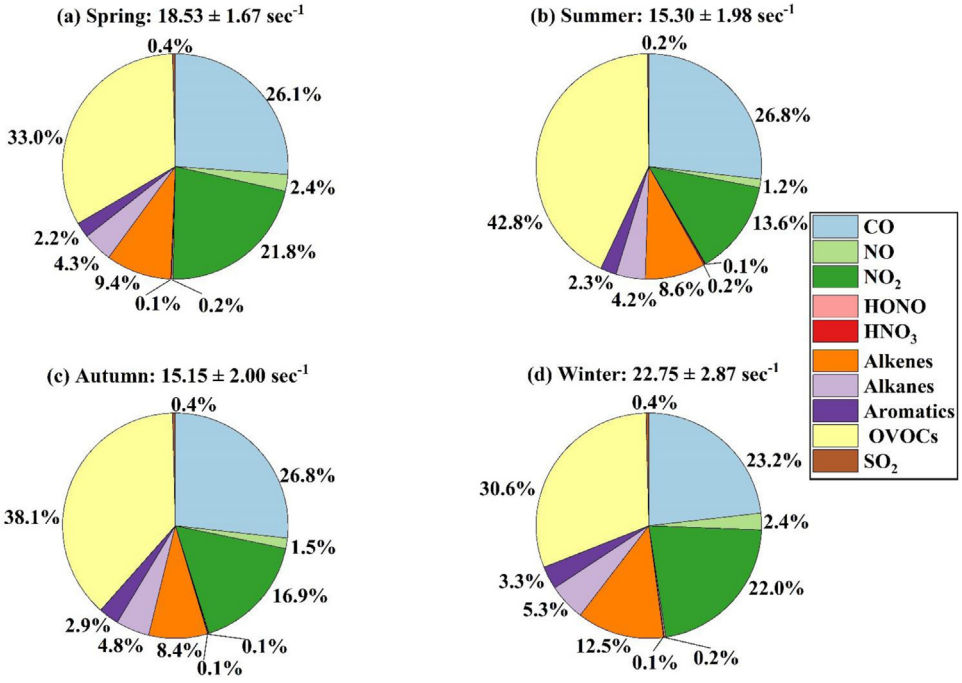

Fig. 4 – The average contributions of different reactants to the total OH reactivity at this observation site in different seasons. (a) Spring, (b) Summer, (c) Autumn, (d) Winter.

OVOCs (20.0%-23.0%), due to the developed transportation system and more traffic vehicles (Tan et al., 2019c). Differently, the contribution of CO was only 11.0%-14.0% in Houston, New York City, Mexico City, significantly lower than that in our study, attributing to higher abundance of CO at the urban site mainly form vehicle emissions (Mao et al., 2010). The research reported that the difference of measured and estimated OH reactivity was attributed to the missing OH reactivity associated with unmeasured and unknown primary and secondary species (Yang et al., 2017; Zhu et al., 2020; Yang et al., 2022). Moreover, related study showed that primary biogenic VOCs and secondary oxidation products may play crucial roles in the missing OH reactivity (Yang et al., 2022). However, unmeasured and unknown primary and secondary species were not considered when calculating the OH reactivity, so the OH reactivity in this study is somewhat underestimated. Except for OH radical, HO_2 and RO_2 radicals might initiate the oxidation of O_3 precursors, promoting photochemical O_3 formation. Thus, it's necessary to discuss RO_x (OH, HO_2, RO_2) chemistry in detail, including the radical initiation, recycling and termination.

2.3. *Radical chemistry*

2.3.1. *Stimulated radical concentrations*

RO_x (OH-HO_2-RO_2) dominated in O_3 photochemistry, and their concentrations in the atmosphere reflect the AOC levels. The mean diurnal profiles of simulated RO_x levels in the daytime (06:00-18:00 LT) in four seasons are presented in Fig. S4, showing that RO_x levels reached the largest at noon in four seasons, in accordance with previous studies in BTH and PRD, where the highest RO_x concentrations were observed at midday (Tan et al., 2018b; Tan et al., 2019b). The average (maximum) daytime concentrations in spring, summer, autumn, winter were (3.51 ± 2.52) (7.07) × 10^6, (8.36 ± 4.74) (14.52) × 10^6, (4.98 ± 3.83) (10.59) × 10^6, (1.35 ± 1.15) (2.95) × 10^6 molec/cm^3 for OH, and (1.05 ± 0.60) (1.94) × 10^8, (4.93 ± 3.21) (9.50) × 10^8, (2.49 ± 1.88) (5.87) × 10^8, (0.42 ± 0.19) (0.78) × 10^8 molec/cm^3 for HO_2, along with (0.53 ± 0.25) (0.88) × 10^8, (2.46 ± 1.37) (4.30) × 10^8, (1.42 ± 0.94) (3.06) × 10^8, (0.22 ± 0.09) (0.33) × 10^8 molec/cm^3 for RO_2, respectively. RO_x levels exhibited obvious seasonal variation characteristics, with a trend of higher level in summer, lower level in winter, medium level in autumn and spring, in consistent with the seasonal variation pattern of the AOC. Due to the lack of observed values in the study area, stimulated RO_x levels were compared with observed RO_x levels in other areas in China. In BTH, daily maximum levels were 17 × 10^6 mol/cm^3 for OH radical, 15 × 10^8 mol/cm^3 for HO_2 radical, and 23 × 10^8 mol/cm^3 for RO_2 radical (Lu et al., 2013; Tan et al., 2017; Tan et al., 2018b). In YRD, daily maximum OH and HO_2 radical levels were 25 × 10^6 and 25 × 10^8 mol/cm^3, respectively (Ma et al., 2022). In PRD, average maximum OH, HO_2, and RO_2 radical concentrations were 16 × 10^6, 15 × 10^8, and 2 × 10^8 mol/cm^3, respectively (Hofzumahaus et al., 2009; Tan et al., 2019a). Totally, stimulated RO_x radical concentrations at the study site were in the range of observed results in other areas in China.

2.3.2. *Radical budget*

In this study, the average diurnal profiles of OH radical production and loss pathways are displayed in Fig. 5. Among the formation pathways of OH, the HO_2 + NO reaction was the most important sources of OH in spring (87.7%), summer (88.0%), autumn (89.3%) and winter (88.1%). The contributions of HONO and O_3 photolysis to OH radical in four seasons are compared (Fig. S5). Photolysis of HONO in winter (7.4%) was more important than O_3 photolysis (2.2%), while O_3 photolysis contributed larger to the production of OH in spring (5.7%), summer (8.9%) and autumn (6.7%). Previous studies showed that O_3 photolysis dominated the OH production under high concentrations of O_3 conditions, whereas HONO photolysis was more important when O_3 concentrations were lower (Ren et al., 2006; Zhu et al., 2020). It should be noted that HONO photolysis dominated OH production in the early morning in spring (before 10:00), summer (before 08:00), autumn (before 09:00) attributed to the accumulation of HONO at night, while photolysis of O_3 were more important in the afternoon due to increased O_3 levels and photolysis rates with the enhancement of photochemical activities, consistent with previous studies in Shanghai (Chan et al., 2017; Zhu et al., 2020). For the OH loss pathways, OH was mainly consumed through OH + VOCs (47.7%-55.2%), followed by OH + CO

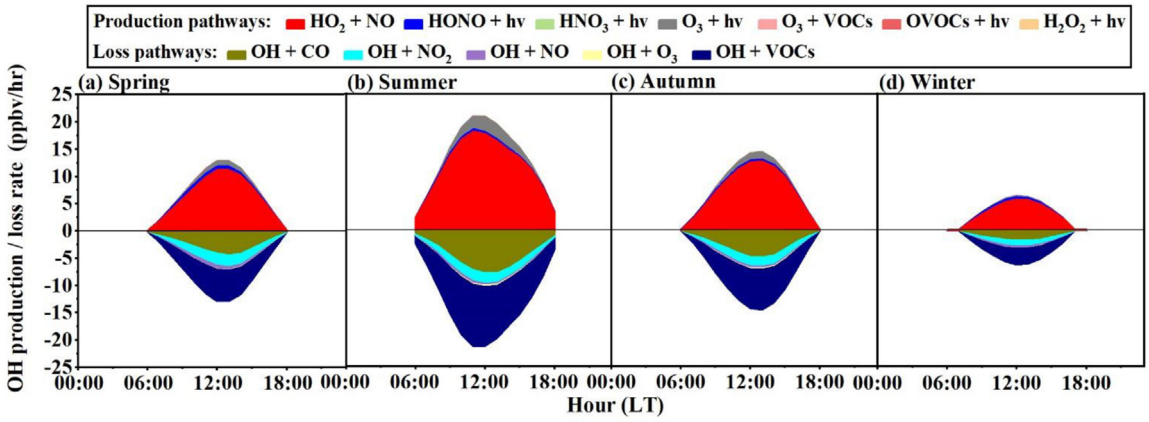

Fig. 5 – The average diurnal profiles of OH production and loss pathways at this observation site in different seasons. (a) Spring, (b) Summer, (c) Autumn, and (d) Winter.

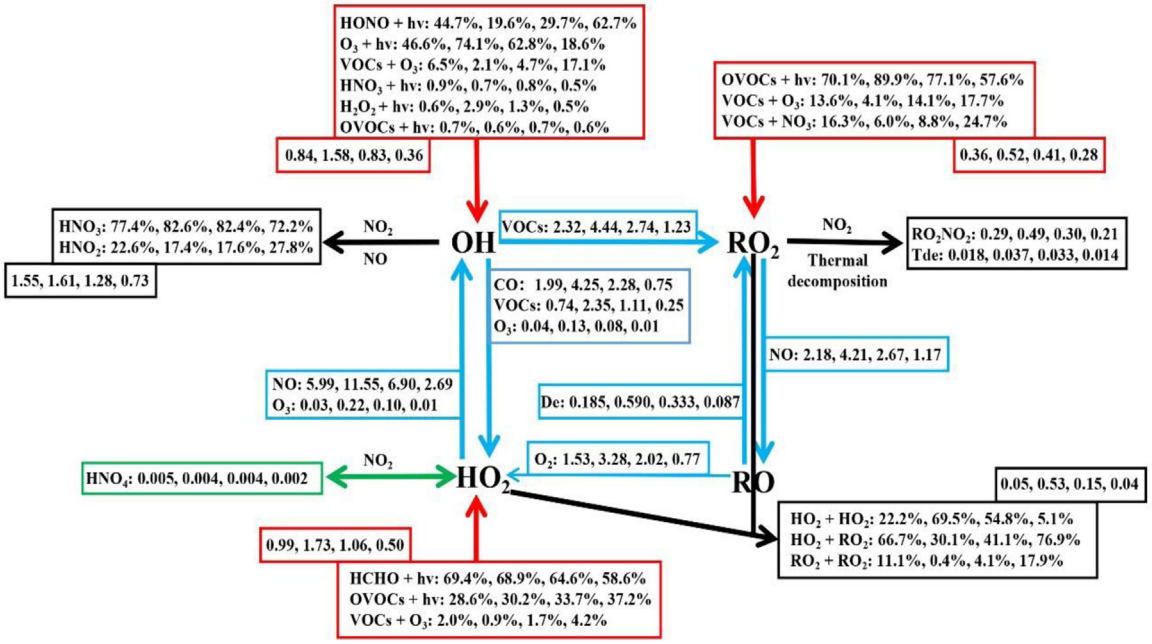

Fig. 6 – Comparison of daytime ROx budget (06:00-18:00 LT) at this observation site in different seasons (units: ppbv/hr). Note: The primary radical sources, radical sinks, radical propagation, and equilibrium between radicals and reservoirs are denoted by red, black, blue, and green lines and boxes, respectively. The numbers from left to right are in the order of spring, summer, autumn, and winter, respectively. The percentages signify the contributions of different reaction pathways to ROx (OH, HO_2, RO_2) budget, and the number values represent for the reaction rates of radical production, loss, propagation, and equilibrium between radicals and reservoirs. (Note: Decomposition (De), Thermal decomposition (Tde))

(24.6%-31.8%), OH + NO_2 (10.0%-17.5%), OH + NO (2.1%-6.6%), and OH + O_3 (0.3%-1.0%), similar with previous studies in five Chinese cities (Beijing, Wuhan, Lanzhou, Chengdu, Shanghai) (Liu et al., 2021).

As the primary sources of HO_2 radical (Fig. S6), photolysis of HCHO is the predominant pathways of HO_2 production in four seasons (10.3%-12.7%), followed by OVOCs photolysis (except for HCHO) (4.3%-7.9%), the reaction of O_3 and VOCs (0.1%-0.9%), similar to that in Xiamen in the southeast of China (Liu et al., 2022b). Besides, the contributions of OH + CO (32.2%-36.8%), RO_2 + NO (31.2%-35.9%), and OH + VOCs (10.6%-19.4%) to the production of HO_2 were very important in four seasons. For the sinks of HO_2, HO_2 + NO was the major loss pathways of HO_2 (93.8%-98.7%) in four seasons, while the contributions of HO_2 + O_3, HO_2 + RO_2, HO_2 + HO_2, HO_2 + NO_2 were limited.

RO_2 production and loss pathways were also analyzed, as shown in Fig. S7. As expected, RO_2 production is dominated by OH + VOCs in four seasons (81.7%-89.5%). OVOCs photolysis was the most important primary formation pathways of RO_2 (9.4%-10.6%). In addition, the reaction of O_3/NO_3 with VOCs contributed moderately to the production of RO_2 (1.0%-4.0%). RO_2 + NOx were the most important sinks of RO_2 (96.8%-98.7%), and the reactions of RO_2 + HO_2/RO_2 for the RO_2 loss is not important, explained by the high abundance of NO_x in the typical urban site affected by transportation emissions. However, in some lower NO_x emission areas, the RO_x sinks were dominated by the radical-radical reactions (Mao et al., 2010; Ling et al., 2014).

In summary, the intensity of the total production and loss rates of RO_x was different in four seasons, with the strongest value in summer, the lowest in winter, the moderate and compared in autumn and spring, reflecting more efficient radical recycling in summer (Fig. 6). The major pathways of RO_x production and loss in different seasons were similar. The primary radical sources in the daytime are dominated by photolysis reactions, including photolysis of HCHO, HONO, O_3, and other OVOCs (except for HCHO), and the radical sinks are the reactions of RO_x + NO_x. Besides, for the radical recycling, the reaction of VOCs, CO with OH promoted the production of HO_2 and RO_2 radical. As a result, $HO_2$and RO_2 radical furtherly reacted with NO, producing OH or RO radicals and accelerated the formation of O_3.

2.4. *In-situ O_3 production photochemistry*

2.4.1. *O_3 production and loss pathways*

In this study, the average diurnal profiles of the net O_3 production rate determined by the OBM simulation in four seasons are shown in Fig. 7. The peak of the net O_3 production rate in summer (19.13 ppbv/hr, with an average daytime value of 14.55 ppbv/hr) was the highest, followed by autumn (13.57 ppbv/hr, with an average value of 8.99 ppbv/hr), spring (11.24 ppbv/hr, with an average value of 7.41 ppbv/hr), winter (6.02 ppbv/hr, with an average value of 3.44 ppbv/hr). However, observed O_3 concentrations in autumn and spring were higher than those in summer and winter at the urban site, significantly differed from that in the North China Plain, where

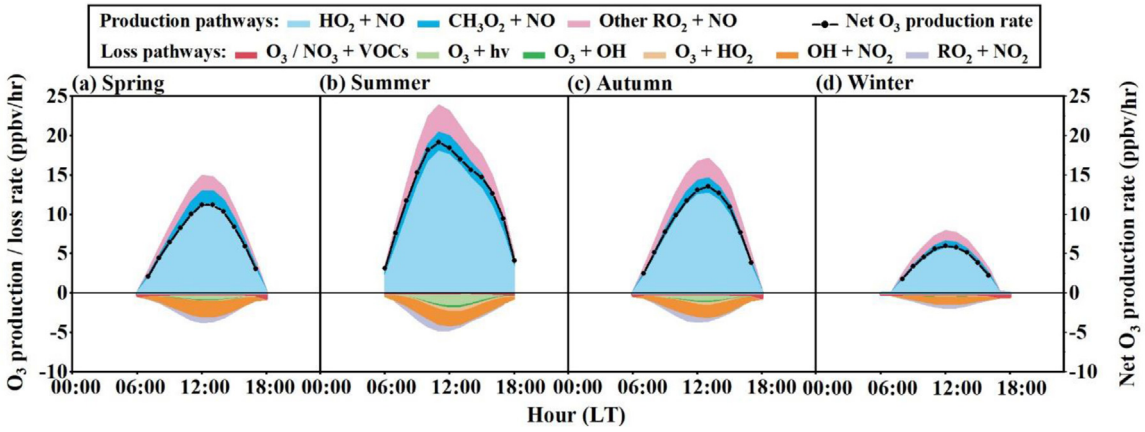

Fig. 7 – The average diurnal profiles of situ O_3 production and loss pathways and net O_3 production rate at this observation site in different seasons. (a) Spring, (b) Summer, (c) Autumn, (d) Winter.

higher O_3 concentrations frequently occurred in summer (Tan et al., 2019c; Wang et al., 2022b). Generally, observed O_3 concentrations depended on the physical process (including horizontal transportation, vertical transportation, and deposition) and the local photochemical production. Therefore, in summer, the favorable photochemical conditions (e.g., strong UV and photolysis rates) were conductive to local O_3 production, but the comprehensive effect of clean oceanic air mass and frequent precipitation at the study area might dilute O_3 concentrations (Zhang et al., 2013). The O_3 production rate in different regions were compared to estimate the ability of local O_3 generate. The daily maximum O_3 production rates were 40 ppbv/hr in Guangzhou, 70 ppbv/hr in Beijing, 28 ppbv/hr in Chengdu (Lu et al., 2012; Lu et al., 2013; Tan et al., 2018a). Even during the serious ozone pollution episode, local O_3 production rate in Guangzhou, Shanghai, Lanzhou was up to 90, 50, 40 ppbv/hr, respectively (Xue et al., 2014). Obviously, the local photochemical O_3 production rate at the study site were lower than those in Chinese megacities, but was compared to the Los Angeles and London (10-20 ppbv/hr) (Griffith et al., 2016; Whalley et al., 2018).

In addition, situ O_3 production and loss pathways were furtherly analyzed (Fig 7). O_3 formation (> 70% for four seasons) was dominated by the reaction of HO_2 + NO, which was the most important formation pathways of OH and thereby initiated the oxidation of VOCs. The second important pathway of O_3 production was the reaction of other RO_2+ NO (13.9%-17.7%), followed by CH_3O_2 + NO (10.6%-12.3%), in agreement with previous work (Ling et al., 2014; Wang et al., 2022b). On the other hand, the dominant loss pathway of O_3 was OH + NO_2 in spring (61.9%), summer (47.8%), autumn (53.8%), and winter (54.1%), and the second prominent pathway of O_3 loss differed in four seasons, RO_2 + NO_2 in spring (14.7%), autumn (15.4%), winter (21.5%), but photolysis of O_3 in summer (21.0%) due to the stronger photolysis rate in summer. O_3 photolysis in spring (10.1%), autumn (13.1%), RO_2 + NO_2 in summer (14.6%), O_3/NO_3 + VOCs in winter (19.1%) were the third important loss pathway of O_3.

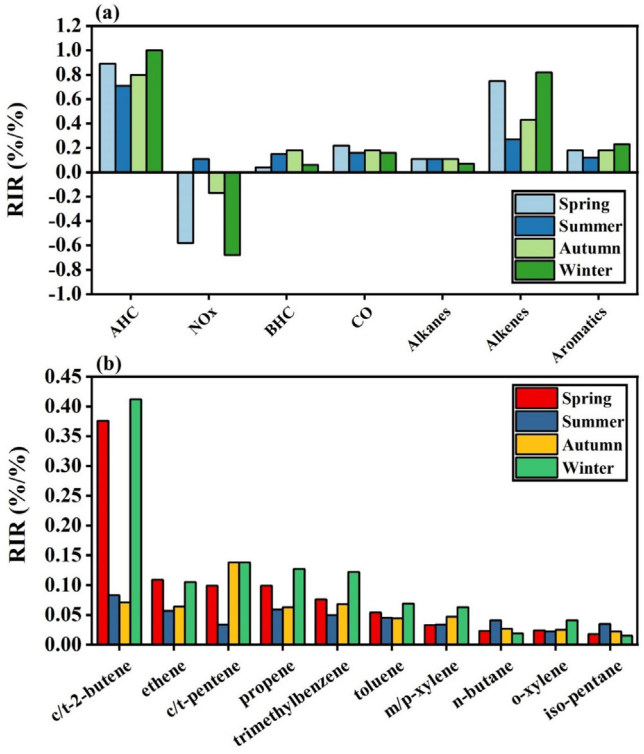

Fig. 8 – The average RIRs of O_3 precursors and major VOC species at this observation site in different seasons (AHC: anthropogenic VOCs; BHC: biogenic VOCs). (a) The RIRs of AHC (including alkanes, alkenes, aromatics), NOx, BHC, CO. (b) The top 10 RIRs of VOC species.

2.4.2. *O_3-NOx-VOCs sensitivities*

In this study, the relative incremental reactivity (RIR) was used to diagnose the sensitivity of O_3 formation to its precursors. Fig. 8a illustrates the average RIR values (RIRs) of O_3 precursors in four seasons. The negative RIRs of NO_x and the positive RIRs of AHC showed that O_3 formation tended to be a VOC-limited

regime in spring, autumn and winter, while the positive RIRs of NO_x and AHC in summer indicated that O_3 formation was controlled by VOCs and NO_x. The RIRs of AHC and NO_x showed a significant seasonal pattern of winter > spring > autumn > summer, but the RIRs of BHC in autumn and summer were higher because BHC emissions were stronger under higher temperature conditions. Therefore, in summer and autumn, it is necessary to strengthen the control of BHC emissions, whereas reducing AHC and NO_x emissions was more predominant in winter and spring. Among O_3 precursors, the RIRs of AHC were the largest, suggesting that the controlling of AHC is efficient to cut down O_3 concentrations in four seasons. As for VOC groups, higher RIRs of alkenes and aromatics indicated that the control of alkenes and aromatics was more important to decrease O_3 concentrations in four seasons. Because O_3 production was more sensitive to VOCs, it is necessary to further determine the influence of individual VOC species on O_3 production (Fig. 8b). The results indicated that c/t-2-butene, ethene, c/t-pentene, propene, toluene, m/p-xylene, and trimethylbenzene contributed the largest to O_3 formation, especially in winter and spring. These VOC species tend to be considered as traffic emissions, introduction production, solvent usage (Shao et al., 2016; Song et al., 2018; Song et al., 2021). Thus, for O_3 pollution control in Ningde, some strict measures should be taken to control traffic emissions, introduction production, solvent usage. Notably, the RIRs of BHC was compared to the RIRs of individual VOC species, such as ethene, even the RIRs of BHC was the largest in summer and autumn. Hence, the importance of the BHC emission control on O_3 production should be valued in summer and autumn.

3.Conclusions

In this study, we analyzed the atmospheric oxidation process, O_3 production pathways and sensitivity using the OBM at an urban site of southeast China in four seasons in 2019. The ability of O_3 production in summer was the strongest, while the average O_3 concentrations in autumn was the highest, due to better effects of dilution and diffusion in summer. The AOC and RO_x production and loss rates presented obvious seasonal patterns, with the maximum value in summer and the minimum value in winter. The OH reactivity in winter was the highest, the lowest in summer, among which OVOCs, CO, NO_2, alkenes were the predominant contributors to the OH radical loss in four seasons. Photolysis of HONO, O_3, HCHO, and other OVOCs were the most important primary RO_x sources, while the main sinks of RO_x were the reaction of RO_x and NO_x in different seasons. O_3 formation was dominated by the reaction of $HO_2 + NO$, whereas O_3 was mainly consumed by the $OH + NO_2$ reaction. O_3 production was a VOC-limited regime in spring, autumn, and winter, but was co-controlled by VOCs and NO_x in summer. Controlling alkene and aromatic species (e.g., isoprene, c/t-2-butene, ethene, c/t-pentene, propene, toluene, m/p-xylene, trimethylbenzene) emissions were more effective to prevent and control O_3 pollution. Overall, this work provided significant variation characteristics of the atmospheric oxidation processes and O_3 formation in different seasons in the coastal city of southeast China with the rapid urbanization.

Declaration of competing interest

The authors declare that they have no known competing financial interests or personal relationships that could have appeared to influence the work reported in this paper.

Acknowledgements

This work was funded by the Cultivating Project of Strategic Priority Research Program of Chinese Academy of Sciences (No. XDPB1903), the Science and Technology Department of Fujian Province (No. 2022L3025), the National Natural Science Foundation of China (No. U22A20578 & 42277091), the Center for Excellence in Regional Atmospheric Environment Project (No. E0L1B20201), the Xiamen Atmospheric Environment Observation and Research Station of Fujian Province, and Fujian Key Laboratory of Atmospheric Ozone Pollution Prevention (Institute of Urban Environment, Chinese Academy of Sciences>).

Supplementary materials

Supplementary material associated with this article can be found, in the online version, at doi:10.1016/j.jes.2022.11.015.

REFERENCES

Chan, K.L., Wang, S., Liu, C., Zhou, B., Wenig, M.O., Saiz-Lopez, A., 2017. On the summertime air quality and related photochemical processes in the megacity Shanghai, China. Sci. Total Environ. 580, 974–983.

Cohen, A.J., Brauer, M., Burnett, R., Anderson, H.R., Frostad, J., Estep, K., et al., 2017. Estimates and 25-year trends of the global burden of disease attributable to ambient air pollution: an analysis of data from the Global Burden of Diseases Study 2015. The Lancet 389, 1907–1918.

Elshorbany, Y.F., Kurtenbach, R., Wiesen, P., Lissi, E., Rubio, M., Villena, G., et al., 2008. Oxidation capacity of the city air of Santiago, Chile. Atmos. Chem. Phys. 8, 19123–19171.

Geyer, A., Alicke, B., Konrad, S., Schmitz, T., Stutz, J., Platt, U., 2001. Chemistry and oxidation capacity of the nitrate radical in the continental boundary layer near Berlin. J. Geophys. Res.: Atmos. 106, 8013–8025.

Griffith, S.M., Hansen, R., Dusanter, S., Michoud, V., Gilman, J., Kuster, W., et al., 2016. Measurements of hydroxyl and hydroperoxy radicals during CalNex-LA: model comparisons and radical budgets. J. Geophys. Res.: Atmos. 121, 4211–4232.

Hofzumahaus, A., Rohrer, F., Lu, K., Bohn, B., Brauers, T., Chang, C.-C., et al., 2009. Amplified trace gas removal in the troposphere. Science 324, 1702–1704.

Kanaya, Y.C., Renqiu Akimoto, H., Fukuda, M., Komazaki, Y., Yokouchi, Y., Koike, M., et al., 2007. Urban photochemistry in central Tokyo: 1. Observed and modeled OH and HO2 radical concentrations during the winter and summer of 2004. J. Geophys. Res.: Atmos. 112.

Li, L., Xie, F., Li, J., Gong, K., Xie, X., Qin, Y., et al., 2022. Diagnostic analysis of regional ozone pollution in Yangtze River Delta, China: a case study in summer 2020. Sci. Total Environ. 812, 151511.

Li, M., Zhang, Q., Zheng, B., Tong, D., Lei, Y., Liu, F., et al., 2019. Persistent growth of anthropogenic non-methane volatile organic compound (NMVOC) emissions in China during 1990–2017: drivers, speciation and ozone formation potential. Atmos. Chem. Phys. 19, 8897–8913.
Li, Z., Xue, L., Yang, X., Zha, Q., Tham, Y.J., Yan, C., et al., 2018a. Oxidizing capacity of the rural atmosphere in Hong Kong. Southern China. Sci. Total Environ. 612, 1114–1122.
Li, Z., Xue, L., Yang, X., Zha, Q., Tham, Y.J., Yan, C., et al., 2018b. Oxidizing capacity of the rural atmosphere in Hong Kong. Southern China. Sci. Total Environ. 612, 1114–1122.
Ling, Z., Guo, H., Lam, S., Saunders, S., Wang, T.J.J.o.G.R.A., 2014. Atmospheric photochemical reactivity and ozone production at two sites in Hong Kong: application of a master chemical mechanism–photochemical box model. J. Geophys. Res.: Atmos. 119, 10567–10582.
Liu, T., Chen, G., Chen, J., Xu, L., Li, M., Hong, Y., et al., 2022a. Seasonal characteristics of atmospheric peroxyacetyl nitrate (PAN) in a coastal city of Southeast China: explanatory factors and photochemical effects. Atmos. Chem. Phys. 22, 4339–4353.
Liu, T., Hong, Y., Li, M., Xu, L., Chen, J., Bian, Y., et al., 2022b. Atmospheric oxidation capacity and ozone pollution mechanism in a coastal city of southeastern China: analysis of a typical photochemical episode by an observation-based model. Atmos. Chem. Phys. 22, 2173–2190.
Liu, X., Guo, H., Zeng, L., Lyu, X., Wang, Y., Zeren, Y., et al., 2021. Photochemical ozone pollution in five Chinese megacities in summer 2018. Sci. Total Environ. 801, 149603.
Liu, X., Qu, H., Huey, L.G., Wang, Y., Sjostedt, S., Zeng, L., et al., 2017. High levels of daytime molecular chlorine and nitryl chloride at a rural site on the North China Plain. Environ. Sci. Technol. 51, 9588–9595.
Lou, S., Holland, F., Rohrer, F., Lu, K., Bohn, B., Brauers, T., et al., 2010. Atmospheric OH reactivities in the Pearl River Delta – China in summer 2006: measurement and model results. Atmos. Chem. Phys. 10, 11243–11260.
Lu, K., Rohrer, F., Holland, F., Fuchs, H., Bohn, B., Brauers, T., et al., 2012. Observation and modelling of OH and HO2 concentrations in the Pearl River Delta 2006: a missing OH source in a VOC rich atmosphere. Atmos. Chem. Phys. 12, 1541–1569.
Lu, K.D., Hofzumahaus, A., Holland, F., Bohn, B., Brauers, T., Fuchs, H., et al., 2013. Missing OH source in a suburban environment near Beijing: observed and modelled OH and HO2 concentrations in summer 2006. Atmos. Chem. Phys. 13, 1057–1080.
Lyu, X., Chen, N., Guo, H., Zhang, W., Wang, N., Wang, Y., et al., 2016. Ambient volatile organic compounds and their effect on ozone production in Wuhan, central China. Environ. Pollut. 541, 200–209.
Lyu, X., Wang, N., Guo, H., Xue, L., Jiang, F., Zeren, Y., et al., 2019. Causes of a continuous summertime O3 pollution event in Jinan, a central city in the North China Plain. Atmos. Chem. Phys. 19, 3025–3042.
Ma, X., Tan, Z., Lu, K., Yang, X., Chen, X., Wang, H., et al., 2022. OH and HO2 radical chemistry at a suburban site during the EXPLORE-YRD campaign in 2018. Atmos. Chem. Phys. 22, 7005–7028.
Mao, J., Ren, X., Chen, S., Brune, W.H., Chen, Z., Martinez, M., et al., 2010. Atmospheric oxidation capacity in the summer of Houston 2006: Comparison with summer measurements in other metropolitan studies. Atmos. Environ. 44, 4107–4115.
Peng, X., Wang, T., Wang, W., Ravishankara, A., George, C., Xia, M., et al., 2022. Photodissociation of particulate nitrate as a source of daytime tropospheric Cl2. Nat. Commun. 13, 1–10.
Qu, H., Wang, Y., Zhang, R., Liu, X., Huey, L.G., Sjostedt, S., et al., 2021. Chemical production of oxygenated volatile organic compounds strongly enhances boundary-layer oxidation chemistry and ozone production. Environ. Sci. Technol. 55, 13718–13727.
Ren, X., Brune, W.H., Mao, J., Mitchell, M.J., Lesher, R.L., Simpas, J.B., et al., 2006. Behavior of OH and HO2 in the winter atmosphere in New York City. Atmos. Environ. 40, 252–263.
Saunders, S.M., Jenkin, M.E., Derwent, R., Pilling, M.J.A.C., 2003. Protocol for the development of the Master Chemical Mechanism, MCM v3 (Part A): tropospheric degradation of non-aromatic volatile organic compounds. Atmos. Chem. Phys. 3, 161–180.
Shao, P., An, J., Xin, J., Wu, F., Wang, J., Ji, D., et al., 2016. Source apportionment of VOCs and the contribution to photochemical ozone formation during summer in the typical industrial area in the Yangtze River Delta, China. Atmos. Res. 176 (177), 64–74.
Song, M., Li, X., Yang, S., Yu, X., Zhou, S., Yang, Y., et al., 2021. Spatiotemporal variation, sources, and secondary transformation potential of volatile organic compounds in Xi'an, China. Atmos. Chem. Phys. 21, 4939–4958.
Song, M., Tan, Q., Feng, M., Qu, Y., Liu, X., An, J., et al., 2018. Source apportionment and secondary transformation of atmospheric nonmethane hydrocarbons in Chengdu, Southwest China. J. Geophys. Res.: Atmos. 123, 9741–9763.
Tan, Z., Fuchs, H., Lu, K., Hofzumahaus, A., Bohn, B., Broch, S., et al., 2017. Radical chemistry at a rural site (Wangdu) in the North China Plain: observation and model calculations of OH, HO2 and RO2 radicals. Atmos. Chem. Phys. 17, 663–690.
Tan, Z., Lu, K., Hofzumahaus, A., Fuchs, H., Bohn, B., Holland, F., et al., 2019a. Experimental budgets of OH, HO2, and RO2 radicals and implications for ozone formation in the Pearl River Delta in China 2014. Atmos. Chem. Phys. 19, 7129–7150.
Tan, Z., Lu, K., Hofzumahaus, A., Fuchs, H., Bohn, B., Holland, F., et al., 2019b. Experimental budgets of OH, HO2, and RO2 radicals and implications for ozone formation in the Pearl River Delta in China 2014. Atmos. Environ. 19, 7129–7150.
Tan, Z., Lu, K., Jiang, M., Su, R., Dong, H., Zeng, L., et al., 2018a. Exploring ozone pollution in Chengdu, southwestern China: a case study from radical chemistry to O3-VOC-NOx sensitivity. Sci. Total Environ. 636, 775–786.
Tan, Z., Lu, K., Jiang, M., Su, R., Wang, H., Lou, S., et al., 2019c. Daytime atmospheric oxidation capacity in four Chinese megacities during the photochemically polluted season: a case study based on box model simulation. Atmos. Chem. Phys. 19, 3493–3513.
Tan, Z., Rohrer, F., Lu, K., Ma, X., Bohn, B., Broch, S., et al., 2018b. Wintertime photochemistry in Beijing: observations of ROx radical concentrations in the North China Plain during the BEST-ONE campaign. Atmos. Chem. Phys. 18, 12391–12411.
Wang, H., Lyu, X., Guo, H., Wang, Y., Zou, S., Ling, Z., et al., 2018a. Ozone pollution around a coastal region of South China Sea: interaction between marine and continental air. Atmos. Chem. Phys. 18, 4277–4295.
Wang, T., Xue, L., Brimblecombe, P., Lam, Y.F., Li, L., Zhang, L., 2017. Ozone pollution in China: a review of concentrations, meteorological influences, chemical precursors, and effects. Sci. Total Environ. 575, 1582–1596.
Wang, W., Yuan, B., Peng, Y., Su, H., Cheng, Y., Yang, S., et al., 2022a. Direct observations indicate photodegradable oxygenated volatile organic compounds (OVOCs) as larger contributors to radicals and ozone production in the atmosphere. Atmos. Chem. Phys. 22, 4117–4128.
Wang, X., Yin, S., Zhang, R., Yuan, M., Ying, Q., 2022b. Assessment of summertime O3 formation and the O3-NOX-VOC sensitivity in Zhengzhou, China using an observation-based model. Sci. Total Environ. 813, 152449.
Wang, Y., Gao, W., Wang, S., Song, T., Gong, Z., Ji, D., et al., 2020. Contrasting trends of PM2.5 and surface-ozone concentrations in China from 2013 to 2017. Natl. Sci. Rev. 7, 1331–1339.

Wang, Y., Guo, H., Zou, S., Lyu, X., Ling, Z., Cheng, H., et al., 2018b. Surface O3 photochemistry over the South China Sea: Application of a near-explicit chemical mechanism box model. Environ. Pollut. 234, 155–166.
Whalley, L.K., Stone, D., Dunmore, R., Hamilton, J., Hopkins, J.R., Lee, J.D., et al., 2018. Understanding in situ ozone production in the summertime through radical observations and modelling studies during the Clean air for London project (ClearfLo). Atmos. Chem. Phys. 18, 2547–2571.
Xu, J., Ma, J.Z., Zhang, X.L., Xu, X.B., Xu, X.F., Lin, W.L., et al., 2011. Measurements of ozone and its precursors in Beijing during summertime: impact of urban plumes on ozone pollution in downwind rural areas. Atmos. Chem. Phys. 11, 12241–12252.
Xue, L., Gu, R., Wang, T., Wang, X., Saunders, S., Blake, D., et al., 2016. Oxidative capacity and radical chemistry in the polluted atmosphere of Hong Kong and Pearl River Delta region: analysis of a severe photochemical smog episode. Atmos. Chem. Phys. 16, 9891–9903.
Xue, L., Wang, T., Gao, J., Ding, A., Zhou, X., Blake, D., et al., 2014. Ground-level ozone in four Chinese cities: precursors, regional transport and heterogeneous processes. Atmos. Chem. Phys. 14, 13175–13188.
Yang, G., Huo, J., Wang, L., Wang, Y., Wu, S., Yao, L., et al., 2022. Total OH reactivity measurements in a suburban site of Shanghai. J. Geophys. Res.: Atmos. 127, e2021JD035981.
Yang, Y., Shao, M., Keßel, S., Li, Y., Lu, K., Lu, S., et al., 2017. How the OH reactivity affects the ozone production efficiency: case studies in Beijing and Heshan, China. Atmos. Chem. Phys. 17, 7127–7142.
Yang, Y., Wang, Y., Huang, W., Yao, D., Zhao, S., Wang, Y., et al., 2021. Parameterized atmospheric oxidation capacity and speciated OH reactivity over a suburban site in the North China Plain: a comparative study between summer and winter. Sci. Total Environ. 773, 145264.
Yang, Y., Wang, Y., Zhou, P., Yao, D., Ji, D., Sun, J., et al., 2020. Atmospheric reactivity and oxidation capacity during summer at a suburban site between Beijing and Tianjin. Atmos. Chem. Phys. 20, 8181–8200.
Zeng, Y., Cao, Y., Qiao, X., Seyler, B.C., Tang, Y.J., 2019. Air pollution reduction in China: Recent success but great challenge for the future. Sci. Total Environ. 663, 329–337.
Zhang, Y., Mao, H., Ding, A., Zhou, D., Fu, C.J.A.E., 2013. Impact of synoptic weather patterns on spatio-temporal variation in surface O3 levels in Hong Kong during 1999–2011. Atmos. Environ. 73, 41–50.
Zhao, Q., Bi, J., Liu, Q., Ling, Z., Shen, G., Chen, F., et al., 2020. Sources of volatile organic compounds and policy implications for regional ozone pollution control in an urban location of Nanjing, East China. Atmos. Chem. Phys. 20, 3905–3919.
Zhu, J., Wang, S., Wang, H., Jing, S., Lou, S., Saiz-Lopez, A., et al., 2020. Observationally constrained modeling of atmospheric oxidation capacity and photochemical reactivity in Shanghai, China. Atmos. Chem. Phys. 20, 1217–1232.